Parameter degeneracies in neutrino oscillation measurement of leptonic *CP* and *T* violation

Hisakazu Minakata*
Department of Physics, Tokyo Metropolitan University, 1-1 Minami-Osawa, Hachioji, Tokyo 192-0397, Japan

Hiroshi Nunokawa†
Instituto de Física Teórica, Universidade Estadual Paulista, Rua Pamplona 145, 01405-900 São Paulo, SP Brazil

Stephen Parke‡
Theoretical Physics Department, Fermi National Accelerator Laboratory, P.O. Box 500, Batavia, Illinois 60510
(Received 20 August 2002; published 27 November 2002)

The measurement of the mixing angle θ_{13}, sign of Δm^2_{13}, and the *CP* or *T* violating phase δ is fraught with ambiguities in neutrino oscillation. In this paper we give an analytic treatment of the paramater degeneracies associated with measuring the $\nu_\mu \to \nu_e$ probability and its *CP* and/or *T* conjugates. For *CP* violation, we give explicit solutions to allow us to obtain the regions where there exist twofold and fourfold degeneracies. We calculate the fractional differences, $(\Delta\theta/\overline{\theta})$, between the allowed solutions which may be used to compare with the expected sensitivities of the experiments. For *T* violation we show that there is always a complete degeneracy between solutions with positive and negative Δm^2_{13} which arises due to a symmetry and cannot be removed by observing one neutrino oscillation probability and its *T* conjugate. Thus there is always a fourfold parameter degeneracy apart from exceptional points. Explicit solutions are also given and the fractional differences are computed. The biprobability *CP*/*T* trajectory diagrams are extensively used to illuminate the nature of the degeneracies.

DOI: 10.1103/PhysRevD.66.093012 PACS number(s): 14.60.Pq, 25.30.Pt

I. INTRODUCTION

The discovery of neutrino oscillation in atmospheric neutrino observation in Super-Kamiokande [1] and the recent accumulating evidence for solar neutrino oscillations [2] naturally suggests neutrino masses and lepton flavor mixing. It is also consistent with the result of the first man-made beam long-baseline accelerator experiment K2K [3]. Given the new realm of lepton flavor mixing whose door has just been opened, it is natural to seek a program of exploring systematically the whole structure of neutrino masses and lepton flavor mixing.

Most probably, the most difficult task in determining the structure of the lepton mixing matrix, the Maki-Nakagawa-Sakata (MNS) matrix [4], is the determination of the *CP* violating phase δ and the simultaneous (or preceding) measurement of $|U_{e3}| = \sin\theta_{13}$. We use in this paper the standard notation for the MNS matrix with $\Delta m^2_{ij} \equiv m^2_j - m^2_i$. The fact that the most recent analyses of the solar neutrino data [5] strongly favor the large mixing angle (LMA) Mikheyev-Smirnov-Wolfenstein (MSW) solution [6] is certainly encouraging for any attempts to measure leptonic *CP* violation.

Since we know that θ_{13} is small, $\sin^2 2\theta_{13} \lesssim 0.1$, due to the constraint imposed by the CHOOZ reactor experiment [7] and we do not know how small it is, there are two different possibilities. Namely, (A) θ_{13} is determined prior to the experimental search for leptonic *CP* violation, or (B) it is not. Case (A) is desirable experimentally. To determine unknown quantities one by one, if possible, is the most sensible way to proceed with minimal danger of picking up fake effects. But since there is no guarantee that case (A) *is* the case, we must prepare for case (B). Even in case (A), experimental determination of θ_{13} always comes with errors, and one must face a similar problem in case B within the experimental uncertainties. Moreover, it is known that determination of θ_{13} in low energy conventional superbeam type experiments suffers from additional intrinsic uncertainty, the one coming from unknown *CP* violating phase δ. See Ref. [8] for further explanation and a possible way of circumventing the problem. Therefore the determination of δ and θ_{13} are inherently coupled with one another.

Even more seriously, it was noticed by Burguet-Castell *et al.* [9] that there exist two sets of degenerate solutions $(\delta_i, \theta^i_{13})$ $(i=1,2)$ even if oscillation probabilities of $P(\nu_\mu \to \nu_e) \equiv P(\nu)$ and its *CP* conjugate, $CP[P(\nu)] \equiv P(\overline{\nu_\mu} \to \overline{\nu_e})$, is accurately measured. They presented an approximate but transparent framework of analyzing the degeneracy problem, which we follow in this paper. It was then recognized in Ref. [10] that the unknown sign of Δm^2_{13} leads to a duplication of the ambiguity, which entails maximal fourfold degeneracy (see below). It was noticed by Barger *et al.* [11] that the fourfold degeneracy is further multiplied by an ambiguity due to approximate invariance of the oscillation probability under the transformation $\theta_{23} \to \pi/2 - \theta_{23}$. A special feature of the degeneracy problem at the oscillation maximum was noted and analyzed in some detail [8,11]. Recently, the first discussion of the problem of parameter degeneracy in *T* violation measurement was given in Ref. [12].

*Email address: minakata@phys.metro-u.ac.jp
†Email address: nunokawa@ift.unesp.br
‡Email address: parke@fnal.gov

Meanwhile, there were some technological progresses in analyzing the interplay between the genuine CP phase and the matter effects in measuring leptonic CP or T violation in neutrino oscillation, the issue much-discussed but still unsettled [13,14]. The authors of Refs. [10] and [12] introduced, respectively, the ''CP and T trajectory diagrams in bi-probability space'' for pictorial representation of CP-violating and CP-conserving phase effects as well as the matter effect in neutrino oscillations. They showed that when these two types of trajectory diagrams are combined it gives a unified graphical representation of neutrino oscillations in matter [12]. We demonstrate in this paper that they provide a powerful tool for understanding and analyzing the problem of parameter degeneracy, as partly exhibited in Refs. [10,11,15].

It is the purpose of this paper to give a completely general treatment of the problem of parameter degeneracy in neutrino oscillations associated with CP and T violation measurements. We elucidate the nature of the degeneracy and determine the region where it occurs, namely, the regions in the P-$CP[P]$ (and P-$T[P]$) biprobability space in which the same-Δm^2_{13}-sign and/or the mixed-Δm^2_{13}-sign degeneracies take place. While partial treatment of the parameter degeneracy has been attempted for CP measurement before [8–11], such general treatment is still lacking. We believe that it is worthwhile to have such an overview of the parameter degeneracy issue to uncover ways of resolving this problem. See [16–19] for recent discussions.

We present the first systematic discussion of parameter degeneracy in T measurement following our previous paper in which we set up the problem [12]. We uncover a new feature of the degeneracy in T measurement. Namely, we show that for a given T trajectory diagram there always exists another T diagram which completely degenerates with the original one and has the opposite sign of Δm^2_{13}. It means that for any given values of $P(\nu)$ and $T[P(\nu)]$ there are two degenerate solutions of $(\delta,\ \theta_{13})$ with a differing sign of Δm^2_{13}. It should be noticed that this is true no matter how large the matter effect, quite contrary to the case of CP measurement. Therefore determination of the signs of Δm^2_{13} is impossible in a single T measurement experiment unless one of the following conditions is met: (a) one of the solutions is excluded, for example, by the CHOOZ constraint, or (b) some additional information, such as energy distribution of the appearance electrons, is added.

We emphasize that a complete understanding of the structure of the parameter degeneracy should be helpful to one who wants to pursue the solution of the ambiguity problem in an experimentally realistic setting. We, however, do not attempt to discuss the $\theta_{23}\leftrightarrow\pi/2-\theta_{23}$ degeneracy. We also do not try to solve the problem of parameter degeneracy exactly though it is in principle possible by using an exact but reasonably compact expression of the oscillation probability obtained by Kimura, Takamura, and Yokomakura [20]. Instead, we restrict ourselves into the treatment with the approximation introduced by Burguet-Castell *et al.* [9] in which the approximate formula for the oscillation probability derived by Cervera *et al.* [21] was employed. Though not exact, it gives us a much more transparent overview of the problem of parameter degeneracy.

II. PROBLEM OF PARAMETER AMBIGUITY IN CP AND T VIOLATION MEASUREMENT

We define the ''CP (T) parameter ambiguity'' as the problem of having multiple solutions of (δ,θ_{13}) and the sign of Δm^2_{23} for a given set of measured values of oscillation probabilities of $P(\nu_\mu\rightarrow\nu_e)$ and its CP (T) conjugate, $CP[P(\nu)]\equiv P(\bar{\nu}_\mu\rightarrow\bar{\nu}_e)$ $(T[P(\nu)]\equiv P(\nu_e\rightarrow\nu_\mu))$. We concentrate in this paper on this channel because precise measurement is much harder in other channels, e.g., in $\nu_e\rightarrow\nu_\tau$. Our use of $\nu_\mu\rightarrow\nu_e$ and its CP conjugate is due to our primary concern on conventional superbeam type experiments [22]. The reader should keep this difference in mind if they try to compare our equations with those in Refs. [9,12] in which they use $\nu_e\rightarrow\nu_\mu$ and its CP conjugate, a natural choice for neutrino factories [21,23]. It should also be noted that the neutrino factories and the superbeam experiments are studying processes which are T conjugates.

In this section we utilize the CP and the T trajectory diagrams introduced in [10] and [12], respectively, to explain what is the problem of parameter ambiguity and to achieve qualitative understanding of the solutions without using equations. But before entering into the details we want to justify, at least partly, our setting, i.e., prior determination of all the remaining parameters besides δ and θ_{13}.

A. Problem of parameter degeneracy; setup of the problem

We assume that at the time that an experiment for measuring (δ,θ_{13}) is carried out all the remaining parameters in the MNS matrix, θ_{23}, $|\Delta m^2_{23}|$, θ_{12}, and Δm^2_{12}, are determined accurately. The discussion on how the experimental uncertainties affect the problem of parameter degeneracy is important, but is beyond the scope of this paper. It should be more or less true, because θ_{23} and Δm^2_{23} will be determined quite accurately by the future long-baseline experiments [24–26] up to the $\theta_{23}\leftrightarrow\pi/2-\theta_{23}$ ambiguity. Most notably, the expected sensitivities in the JHF-SK experiment in its phase I are [24]

$$\delta(\sin^2 2\theta_{23})\simeq 10^{-2},$$
$$\delta(|\Delta m^2_{23}|)\simeq(4-6)\times 10^{-5}\ \text{eV}^2 \qquad (1)$$

at around $|\Delta m^2_{23}|=3\times 10^{-3}$ eV^2. On the other hand, the best place for accurate determination of θ_{12} and Δm^2_{12}, assuming the LMA MSW solar neutrino solution, is most probably the KamLAND experiment; the expected sensitivities are [27]

$$\delta(\tan^2\theta_{12})\simeq 10\%,$$
$$\delta(\Delta m^2_{12})\simeq 10\% \qquad (2)$$

at around the LMA best fit parameters. Therefore we feel that our setting, prior determination of all the mixing angles and Δm^2's besides δ, θ_{13}, and the sign of Δm^2_{23}, is a reasonable one at least in the first approximation.

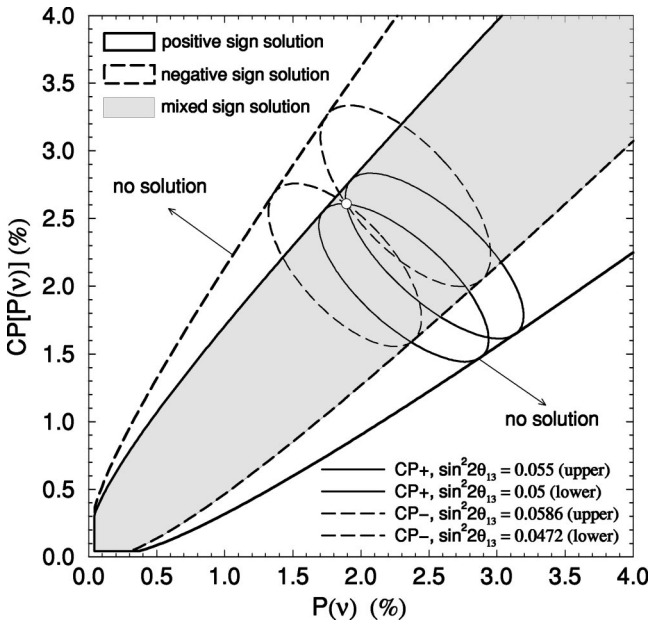

FIG. 1. An example of the degenerate solutions for the CERN-Frejius project in the $P(\nu)\equiv P(\nu_\mu\rightarrow\nu_e)$ versus $CP[P(\nu)]\equiv P(\overline{\nu}_\mu\rightarrow\overline{\nu}_e)$ plane. Between the solid (dashed) lines is the allowed region for positive (negative) Δm^2_{13} and the shaded region is where solutions for both signs are allowed. The solid (dashed) ellipses are for positive (negative) Δm^2_{13} and they all meet at a single point. This is the CP parameter degeneracy problem. We have used a fixed neutrino energy of 250 MeV and a baseline of 130 km. The mixing parameters are fixed to be $|\Delta m^2_{13}|=3\times10^{-3}$ eV^2, $\sin^2 2\theta_{23}=1.0$, $\Delta m^2_{12}=+5\times10^{-5}$ eV^2, $\sin^2 2\theta_{12}=0.8$, and $Y_e\rho=1.5$ g cm^{-3}.

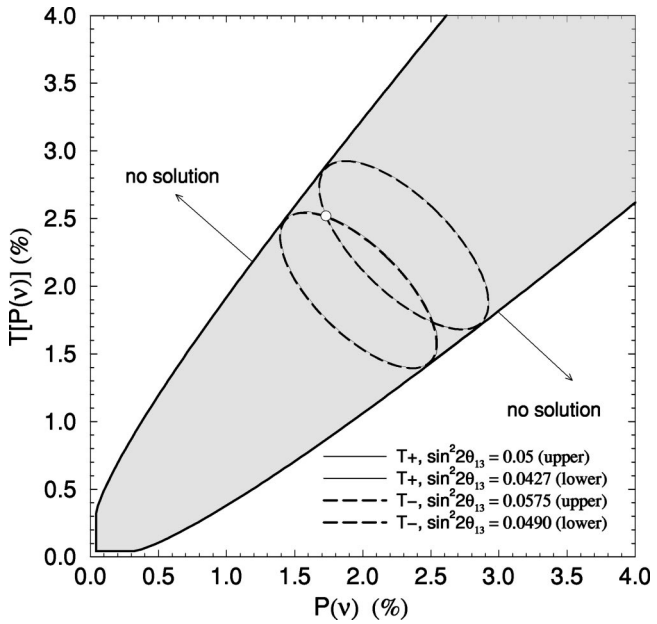

FIG. 2. An example of the degenerate solutions using the energy and path length of the CERN-Frejius project in the $P(\nu)\equiv P(\nu_\mu\rightarrow\nu_e)$ versus $T[P(\nu)]\equiv P(\nu_e\rightarrow\nu_\mu)$ plane. For this figure there is complete overlap in the region (shaded) that allows solutions for either sign of Δm^2_{13}. The solid (dashed) ellipses are for positive (negative) Δm^2_{13} and they all meet at the "measured point," $(P,P^T)=(1.7,2.5)\%$. This is the T-parameter degeneracy problem. Notice that for the each ellipse with positive Δm^2_{13} there is a completely degenerate ellipse with negative Δm^2_{13}. This feature will be explained in Sec. III C. Parameters are the same as in Fig. 1.

B. Pictorial representation of parameter ambiguities

In this section we use CP and the T trajectory diagrams [10,12] to explain intuitively what is the problem of parameter degeneracy, and to achieve qualitative understanding of the solutions without using equations. In Fig. 1 we display four CP trajectories in the P-$CP[P]$ biprobability space which all have intersections at $P(\nu)=1.9\%$ and $CP[P(\nu)]=2.6\%$. The four CP trajectories are drawn with four different values of θ_{13}, $\sin^2 2\theta_{13}=0.055$, 0.050, 0.586, and 0.472, and the former (latter) two trajectories correspond to positive (negative) Δm^2_{13}. The analytic expressions of the four degenerate solutions will be derived in Sec. IV. The neutrino energy E and the baseline length L are taken as $E=250$ MeV and $L=130$ km, respectively.[1] The setting anticipates an application to the CERN-Frejius project [28], where the regions with parameter ambiguities are widest. The values of all the remaining mixing parameters are given in the caption of Fig. 1.

Figure 1 demonstrates that there is a fourfold degeneracy in the determination of $(\delta,\ \theta_{13})$ for a given set of $P(\nu)$ and $CP[P(\nu)]$. The region between the solid lines and the region between the dashed lines in Fig. 1 are the regions where twofold degeneracies exist in the solutions of $(\delta,\ \theta_{13})$ for positive and negative Δm^2_{13} sectors, respectively. [See Eq. (48) in Sec. IV.] It is intuitively understandable that the region where degenerate solutions exists is the region swept over by the CP trajectories when the parameter θ_{13} is varied, while keeping other mixing parameters and the experimental conditions fixed. The shaded region is the region where the full fourfold degeneracy exists.

Now we turn to the T measurement. In Fig. 2 we display four T trajectories in the P-$T[P]$ biprobability space which all have intersections at $P(\nu)=1.7\%$ and $T[P(\nu)]=2.5\%$. The four T trajectories are drawn with four different values of θ_{13}, $\sin^2 2\theta_{13}=0.05$, 0.0427, 0.575, and 0.490, and the former (latter) two trajectories correspond to positive (negative) Δm^2_{13}. Matter effects split the positive and negative Δm^2_{13} trajectories, see [12], thus different values of θ are required for mixed-sign trajectories to overlap. The remaining mixing parameters and the experimental setting are the same as in Fig. 1.

A clear and interesting difference from the CP diagram manifests itself already at this level, reflecting the highly symmetric nature of the T conjugate probabilities as will be made explicit in Eq. (3). Namely, the two different-Δm^2_{13}-sign diagrams (the first and the third, and the second and fourth) completely overlap with each other. In the next section we will make it clear that the complete degeneracy

[1]In all the figures of this paper we do not average over neutrino energy distributions as was performed in Refs. [10,12] but use a fixed neutrino energy specified for each figure.

originates from a symmetry. Therefore discrimination of the sign of Δm^2_{13} is impossible in a single T violation measurement experiment unless one of the solutions is excluded by another experiment. We will demonstrate in Sec. III that the degeneracy is not an accidental one specific to this particular case, but its existence is generic. There is always a fourfold degeneracy in T measurement.

III. PARAMETER DEGENERACY IN T VIOLATION MEASUREMENTS

We start by presenting an analytic treatment of the problem of parameter degeneracy in T violation measurements primarily because it is simpler and instructive. To do this we generalize the formalism developed by Burguet-Castell *et al.* [9] by treating the cases of positive and negative Δm^2_{13} simultaneously. It provides the basis of our treatment of the degeneracy between the same as well as across the alternating Δm^2_{13}-sign probabilities. It will become clear from the following discussions that the treatment of the mixed-sign degenerate solutions, for both CP and T measurements, can be done as a straightforward generalization of the same-sign degeneracy case by simply taking account of duplication due to the alternating sign of Δm^2_{13} [10].

There are four basic equations satisfied by the T conjugate probabilities in the case of T measurement for small $\sin\theta_{13}$:

$$
\begin{aligned}
P(\nu)_+ &= X_+\theta^2 + Y_+\theta\cos\left(\delta + \frac{\Delta_{13}}{2}\right) + P_\odot ,\\
T[P(\nu)]_+ \equiv P^T(\nu)_+ &= X_+\theta^2 + Y_+\theta\cos\left(\delta - \frac{\Delta_{13}}{2}\right) + P_\odot ,\\
P(\nu)_- &= X_-\theta^2 + Y_-\theta\cos\left(\delta - \frac{\Delta_{13}}{2}\right) + P_\odot ,\\
T[P(\nu)]_- \equiv P^T(\nu)_- &= X_-\theta^2 + Y_-\theta\cos\left(\delta + \frac{\Delta_{13}}{2}\right) + P_\odot ,
\end{aligned}
\tag{3}
$$

where $X_\pm$ and $Y_\pm$ are given in the Appendix, $P_\odot$ indicates the term which is related with solar neutrino oscillations, and $\Delta_{13} \equiv |\Delta m^2_{13}| L/2E$. Note that $\pm$ here refers to the sign of Δm^2_{13} and θ is an abbreviation of $\theta_{13} \simeq \sin\theta_{13}$. In the next sections we discuss the possible solutions for θ and δ for a given measurement of both P and P^T for both the positive and negative sign of Δm^2_{13}.

A. The same-sign degeneracy; T measurement

The treatment in this section applies for two overlapping T trajectories with the same sign of Δm^2_{13}. The degeneracy associated with alternating-sign trajectories will be explored in the next section.

There are two sets of approximate solutions of Eq. (3), θ_i and δ_i, where $(i=1,2)$ and $(i=3,4)$ denotes the solutions in the positive and negative Δm^2_{13} sectors, respectively. They are

$$
\begin{aligned}
\theta_i &= \sqrt{\frac{P - P_\odot}{X_\pm}} - \frac{Y_\pm}{2X_\pm}\cos\left(\delta_i \pm \frac{\Delta_{13}}{2}\right),\\
\theta_i &= \sqrt{\frac{P^T - P_\odot}{X_\pm}} - \frac{Y_\pm}{2X_\pm}\cos\left(\delta_i \mp \frac{\Delta_{13}}{2}\right),
\end{aligned}
\tag{4}
$$

where $\pm$ correspond to solutions in positive and negative Δm^2_{13} sectors.[2] We then obtain, e.g., for the positive Δm^2_{13} sector

$$
\begin{aligned}
\theta_2 - \theta_1 = -\frac{Y_+}{2X_+}\Bigg[&(\cos\delta_2 - \cos\delta_1)\cos\left(\frac{\Delta_{13}}{2}\right)\\
&-(\sin\delta_2 - \sin\delta_1)\sin\left(\frac{\Delta_{13}}{2}\right)\Bigg],
\end{aligned}
$$

$$
\begin{aligned}
\theta_2 - \theta_1 = -\frac{Y_+}{2X_+}\Bigg[&(\cos\delta_2 - \cos\delta_1)\cos\left(\frac{\Delta_{13}}{2}\right)\\
&+(\sin\delta_2 - \sin\delta_1)\sin\left(\frac{\Delta_{13}}{2}\right)\Bigg],
\end{aligned}
\tag{5}
$$

which entails the degeneracy that if (θ_1, δ_1) is a solution so is

$$
\theta_2 = \theta_1 + \frac{Y_+}{X_+}\cos\delta_1\cos\left(\frac{\Delta_{13}}{2}\right) \quad \text{and} \quad \delta_2 = \pi - \delta_1 , \tag{6}
$$

in addition to the trivial solution. A similar degeneracy also holds for the negative Δm^2_{13} sector, that is, if (θ_3, δ_3) is a solution so is

$$
\theta_4 = \theta_3 + \frac{Y_-}{X_-}\cos\delta_3\cos\left(\frac{\Delta_{13}}{2}\right) \quad \text{and} \quad \delta_4 = \pi - \delta_3 . \tag{7}
$$

Both of these same sign Δm^2_{13} degeneracies are in matter though they look like the vacuum degeneracies as discussed in [10]. Notice that if the experimental setup is chosen such that $\cos(\Delta_{13}/2) = 0$ [8] or nature has chosen $\cos\delta = 0$ then the same-sign degeneracies are removed.

B. The mixed-sign degeneracy; T measurement

Let us now examine the problem of parameter degeneracy which involves positive and negative Δm^2_{13}. The basic equations (3) can be approximately solved for the mixed-sign situation as

[2]The above solutions are exact solutions to the system of Eq. (3) if we were to add terms $Y^2_\pm \cos^2(\delta \pm \Delta_{13}/2)/(4X_\pm)$ to the equations, (3). In what follows we have systematically ignored terms of $\mathcal{O}(Y^2_\pm/X_\pm)$.

$$\theta_1 = \sqrt{\frac{P-P_\odot}{X_+}} - \frac{Y_+}{2X_+}\cos\left(\delta_1 + \frac{\Delta_{13}}{2}\right),$$

$$\theta_1 = \sqrt{\frac{P^T-P_\odot}{X_+}} - \frac{Y_+}{2X_+}\cos\left(\delta_1 - \frac{\Delta_{13}}{2}\right), \tag{8}$$

$$\theta_3 = \sqrt{\frac{P-P_\odot}{X_-}} - \frac{Y_-}{2X_-}\cos\left(\delta_3 - \frac{\Delta_{13}}{2}\right),$$

$$\theta_3 = \sqrt{\frac{P^T-P_\odot}{X_-}} - \frac{Y_-}{2X_-}\cos\left(\delta_3 + \frac{\Delta_{13}}{2}\right). \tag{9}$$

We will now exactly determine θ and δ using the above set of approximate solutions, (8) and (9), as our starting point. First,

$$\sin\delta_1 \sin\frac{\Delta_{13}}{2} = -\frac{\sqrt{X_+}}{Y_+}\left(\sqrt{P-P_\odot} - \sqrt{P^T-P_\odot}\right), \tag{10}$$

$$\sin\delta_3 \sin\frac{\Delta_{13}}{2} = \frac{\sqrt{X_-}}{Y_-}\left(\sqrt{P-P_\odot} - \sqrt{P^T-P_\odot}\right) \tag{11}$$

and $\cos\delta_i$ is given by $\cos\delta_i = \pm\sqrt{1-\sin^2\delta_i}$. Using these $\cos\delta_i$ the values of θ are given by

$$\theta_1 = \frac{\left(\sqrt{P-P_\odot} + \sqrt{P^T-P_\odot}\right)}{2\sqrt{X_+}} - \frac{Y_+}{2X_+}\cos\delta_1\cos\frac{\Delta_{13}}{2}, \tag{12}$$

$$\theta_3 = \frac{\left(\sqrt{P-P_\odot} + \sqrt{P^T-P_\odot}\right)}{2\sqrt{X_-}} - \frac{Y_-}{2X_-}\cos\delta_3\cos\frac{\Delta_{13}}{2}. \tag{13}$$

To relate these alternating sign solutions we use the identity, see the Appendix,

$$\frac{\sqrt{X_+}}{Y_+} = -\frac{\sqrt{X_-}}{Y_-}, \tag{14}$$

derivable under the Cervera *et al.* approximation.[3] Then, it follows that

$$\sin\delta_1 = \sin\delta_3,$$

$$(\cos\delta_1 + \cos\delta_3)\cos\frac{\Delta_{13}}{2} = -2\frac{\sqrt{X_+}}{Y_+}\left(\sqrt{X_+}\theta_1 - \sqrt{X_-}\theta_3\right). \tag{15}$$

One can choose without loss of generality $\delta_3 = \pi - \delta_1$ as a solution of Eq. (15). Then, for a given P and P^T measurement, apart from (θ_1, δ_1) there are three other solutions[4] given by

$$\theta_2 = \theta_1 + \frac{Y_+}{X_+}\cos\delta_1\cos\left(\frac{\Delta_{13}}{2}\right) \text{ and } \delta_2 = \pi - \delta_1,$$

$$\theta_3 = \sqrt{\frac{X_+}{X_-}}\theta_1 \text{ and } \delta_3 = \pi - \delta_1, \tag{16}$$

$$\theta_4 = \theta_3 - \frac{Y_-}{X_-}\cos\delta_1\cos\left(\frac{\Delta_{13}}{2}\right) \text{ and } \delta_4 = \delta_1.$$

Therefore there is no ambiguity in the determination of δ in T violation measurement apart from the one $\delta \to \pi - \delta$ independent of the sign of Δm^2_{13}. Fortunately, this degeneracy does not obscure existence or nonexistence of leptonic T (or CP) violation. This feature arises because of the highly constrained nature of system (3) of T conjugate probabilities.

The physically allowed region of the T diagram is determined by the constraint that $\sin^2\delta_i \leqslant 1$ which in terms of P and P^T is

$$\left(\sqrt{P-P_\odot} - \sqrt{P^T-P_\odot}\right)^2 \leqslant \frac{Y_+^2}{X_+}\sin^2\left(\frac{\Delta_{13}}{2}\right) = \frac{Y_-^2}{X_-}\sin^2\left(\frac{\Delta_{13}}{2}\right) \tag{17}$$

and is the same region for both signs of Δm^2_{13} because of the identity Eq. (14). In Fig. 2, this region is the shaded region using the CERN-Frejius parameters. At the boundary of the allowed physical region $\cos\delta = 0$ and the same-sign degeneracy vanishes, however, the opposite sign degeneracy is nonzero.

We define the fractional differences, $\Delta\theta/\overline{\theta}$, by

$$\left(\frac{\Delta\theta}{\overline{\theta}}\right)_{ij} \equiv \frac{\theta_i - \theta_j}{(\theta_i + \theta_j)/2}, \tag{18}$$

to quantify how different the two degenerate solutions are. In fact, one can obtain simple expressions for the various fractional differences:

$$\left(\frac{\Delta\theta}{\overline{\theta}}\right)_{12} = \left(\frac{\Delta\theta}{\overline{\theta}}\right)_{34} = \frac{-2Y_+\cos\delta_1\cos\left(\frac{\Delta_{13}}{2}\right)}{\sqrt{X_+}\left(\sqrt{P-P_\odot} + \sqrt{P^T-P_\odot}\right)}, \tag{19}$$

$$\left(\frac{\Delta\theta}{\overline{\theta}}\right)_{31} = \left(\frac{\Delta\theta}{\overline{\theta}}\right)_{42} = 2\frac{\left(\sqrt{X_+} - \sqrt{X_-}\right)}{\left(\sqrt{X_+} + \sqrt{X_-}\right)}, \tag{20}$$

[3]Unless Eq. (14) holds we get into trouble because then Eqs. (8) or (9) do not allow the (same-sign) solution $\theta_1 = \theta_2$ and $\delta_1 = \delta_2$, which must exist as shown in Ref. [12]. Therefore use of the formula of oscillation probability obtained by Cervera *et al.* who summed up all order matter effect is essential.

[4]As a convention, we have chosen $\cos\delta_1 \leqslant 0$ so that for $\Delta_{13} \leqslant \pi$, $\theta_1 \geqslant \theta_2$ and $\theta_3 \geqslant \theta_4$.

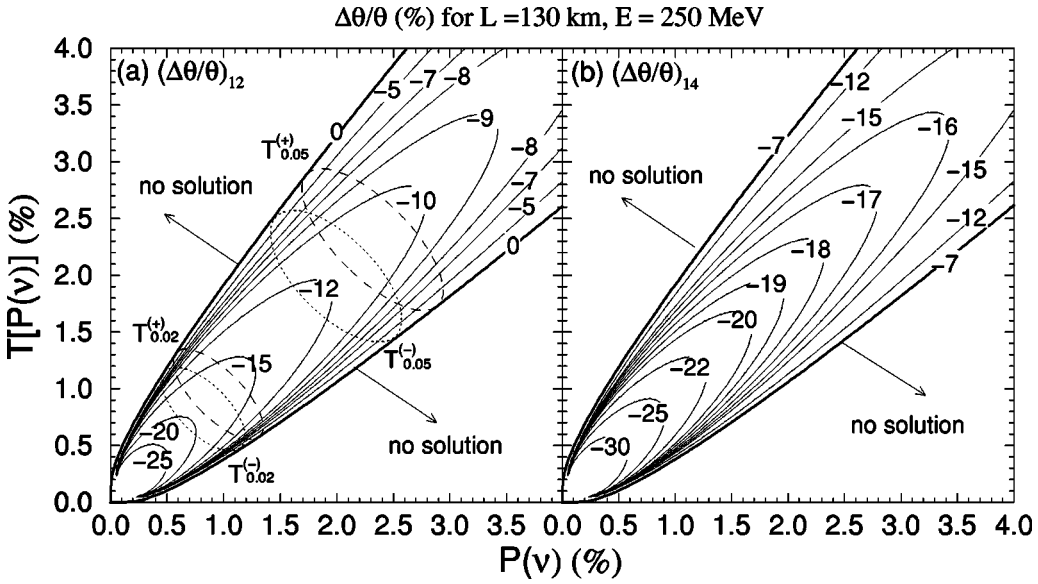

FIG. 3. The isofractional differences, as a percent, for the allowed solutions for the mixing angle θ_{13} in the $P(\nu)\equiv P(\nu_\mu\rightarrow\nu_e)$ versus $T[P(\nu)]\equiv P(\nu_e\rightarrow\nu_\mu)$ plane for the CERN-Frejius project. The fractional differences for solutions (3,4) is identical to that for (1,2) and the fractional difference for (3,2) equals the fractional difference for (1,4) plus or minus a constant, see Eqs. (19)–(22). In this case the fractional difference (3,2) has a zero contour. The parameters are the same as in Fig. 1. The ellipses are labeled $T^{(\pm)}_{\sin^2 2\theta_{13}}$ to show the relevant size of $\sin^2 2\theta_{13}$ for this figure.

$$\left(\frac{\Delta\theta}{\overline{\theta}}\right)_{14}\approx\frac{-2Y_+\cos\delta_1\cos\left(\frac{\Delta_{13}}{2}\right)}{\sqrt{X_+}\left(\sqrt{P-P_\odot}+\sqrt{P^T-P_\odot}\right)}-2\left(\frac{\sqrt{X_+}-\sqrt{X_-}}{\sqrt{X_+}+\sqrt{X_-}}\right),\tag{21}$$

$$\left(\frac{\Delta\theta}{\overline{\theta}}\right)_{32}\approx\frac{-2Y_+\cos\delta_1\cos\left(\frac{\Delta_{13}}{2}\right)}{\sqrt{X_+}\left(\sqrt{P-P_\odot}+\sqrt{P^T-P_\odot}\right)}+2\left(\frac{\sqrt{X_+}-\sqrt{X_-}}{\sqrt{X_+}+\sqrt{X_-}}\right).\tag{22}$$

The same sign fractional difference, (1,2) and (3,4), decreases with increasing P and P^T and thus θ, whereas the first mixed-sign fractional difference, (3,1) and (4,2), is independent of the size of P and P^T and thus θ. The second and third mixed-sign fractional differences, (1,4) and (2,3), are similar to the same-sign fractional difference but offset by an energy dependent constant. The relationship between the fractional difference in the measured quantity $\sin^2 2\theta$ and θ is simply

$$\frac{\sin^2 2\theta_i-\sin^2 2\theta_j}{(\sin^2 2\theta_i+\sin^2 2\theta_j)/2}\approx 2\frac{\theta_i-\theta_j}{(\theta_i+\theta_j)/2}=2\left(\frac{\Delta\theta}{\overline{\theta}}\right)_{ij}\tag{23}$$

for $1\geqslant\theta_i,\theta_j\geqslant|\theta_i-\theta_j|$.

In Figs. 3–5 we have plotted the differences in the allowed θ solutions divided by half the sum for the CERN-Frejius, JHF-SK, and Fermilab-NUMI [29] possible experiments using $\nu_\mu\rightarrow\nu_e$ and its T conjugate $\nu_e\rightarrow\nu_\mu$. The regions where this fractional difference is small are regions where the parameter degeneracy inherent in such measurements is only important once the experimental resolution on θ for a fixed solution is of the same size or smaller. Notice that near the boundaries on the allowed region the fractional differences are small for the same-sign solutions. For the mixed sign, either the (1,4) or (3,2) fractional difference plots have a line for which the fractional difference is zero. This line can be understood as follows: for a given small value of θ the positive and negative Δm^2_{13} ellipses overlap and intersect at two points. As θ varies these intersection points give us this line with zero mixed-sign fractional difference.

C. Symmetry between the two alternating-Δm^2_{13}-sign T diagrams

The observant reader will notice that there is in a general one-to-one correspondence between the solutions with positive Δm^2_{13}, labeled 1 and 2, and those solutions with negative Δm^2_{13}, labeled 3 and 4, in Eq. (16) by using the identity, Eq. (14). In fact this correspondence applies not only to the solutions but to the complete T diagram. For a given T trajectory with positive Δm^2_{13} there always exists a T trajectory with negative Δm^2_{13} with a different value of θ, which nevertheless completely overlaps the positive trajectory, see Fig. 2. This surprising phenomenon occurs because there exists a symmetry in the T probability system defined in Eq. (3).

One can observe from Eq. (3) that a positive Δm^2_{13} trajectory which is defined by the first two equations of Eq. (3) can

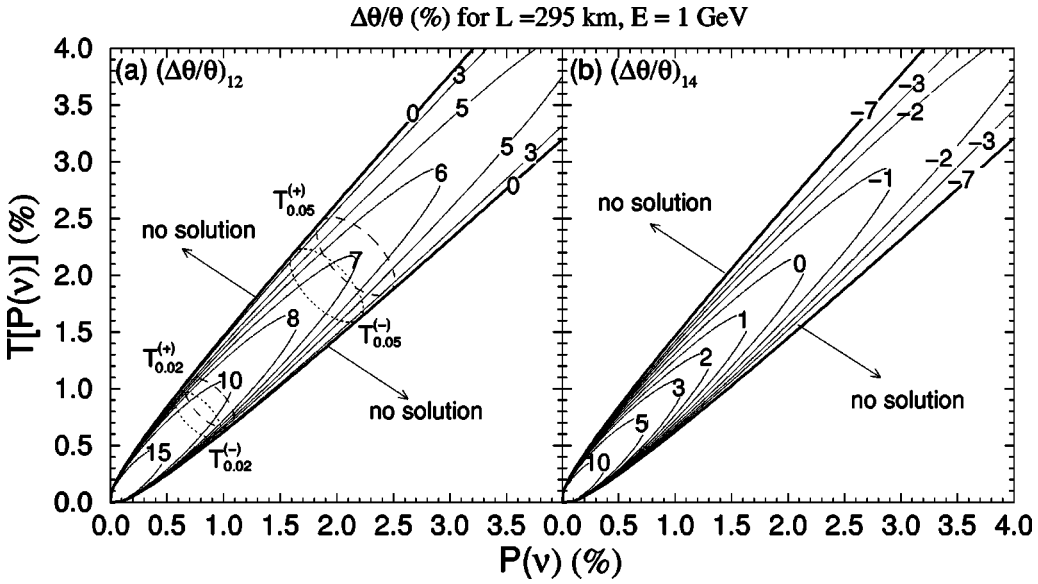

FIG. 4. The isofractional differences, as a percent, for the allowed solutions for the mixing angle θ_{13} in the $P(\nu)\equiv P(\nu_\mu\rightarrow\nu_e)$ versus $T[P(\nu)]\equiv P(\nu_e\rightarrow\nu_\mu)$ plane for the JHK-SK project. The fractional differences for solutions (3,4) is identical to that for (1,2) and the fractional difference for (3,2) equals the fractional difference for (1,4) plus or minus a constant, see Eqs. (19)–(22). The zero contour appearing in the (1,4) fractional difference is explained in the text. The parameters are the same as in Fig. 1. The ellipses are labeled as in Fig. 3.

be used to generate a negative Δm^2_{13} trajectory which completely overlaps with the original one by the transformation

$$\delta\rightarrow\pi-\delta,$$

$$\theta\rightarrow\sqrt{\frac{X_-}{X_+}}\theta. \tag{24}$$

This means that for a measure set of P and P^T there are always two sets of solutions with a different sign of Δm^2_{13}. There is no way to resolve this ambiguity because the two T trajectories are completely degenerate. It should be noticed that this situation occurs no matter how large a matter effect at a much longer baseline. In such a case, two T trajectories with the same θ_{13} but opposite sign of Δm^2_{13} are far apart,

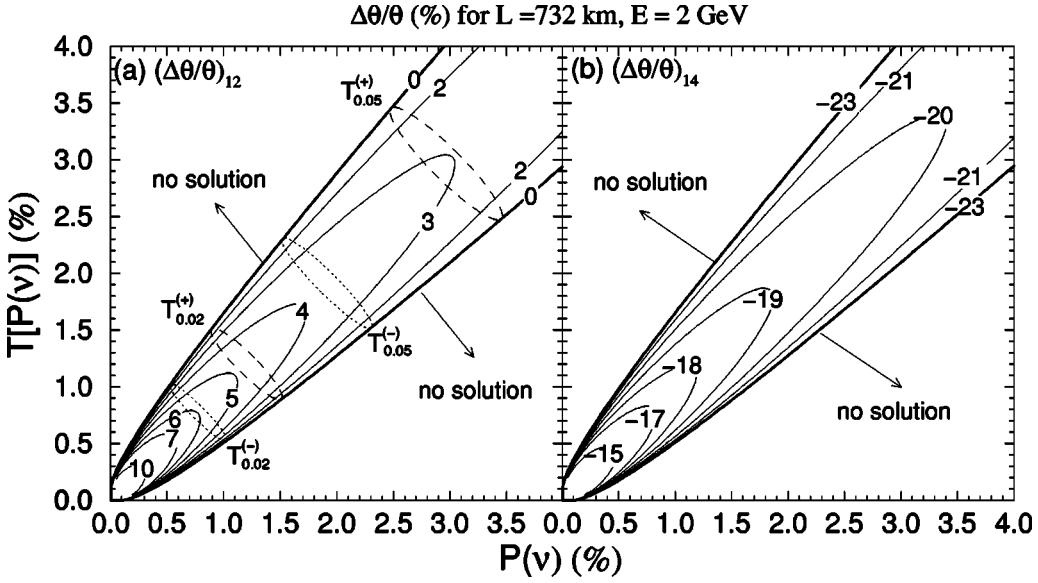

FIG. 5. The isofractional differences, as a percent, for the allowed solutions for the mixing angle θ_{13} in the $P(\nu)\equiv P(\nu_\mu\rightarrow\nu_e)$ versus $T[P(\nu)]\equiv P(\nu_e\rightarrow\nu_\mu)$ plane for the Fermilab-NUMI project. The fractional differences for solutions (3,4) is identical to that for (1,2) and the fractional difference for (3,2) equals the fractional difference for (1,4) plus or minus a constant, see Eqs. (19)–(22). At very small probability the (1,4) fractional difference has a zero contour. The parameters are the same as in Fig. 1. The ellipses are labeled as in Fig. 3.

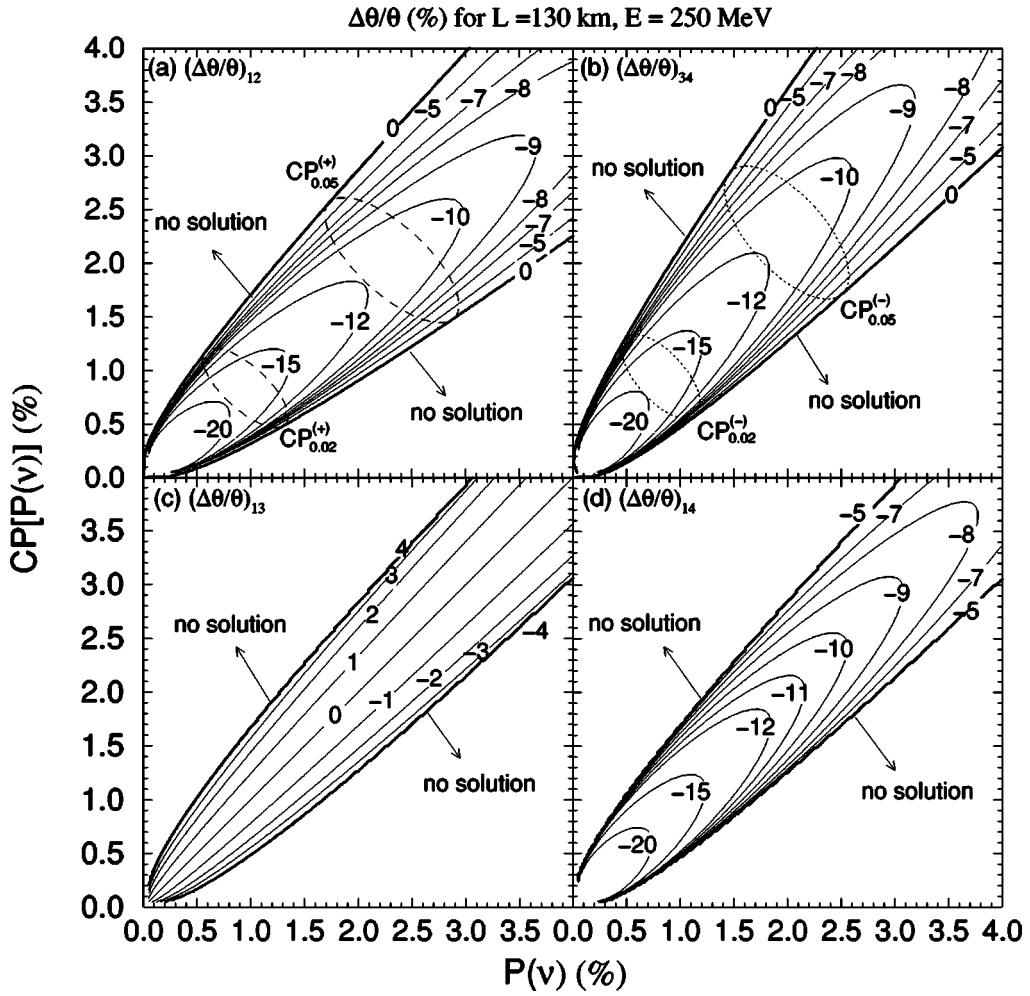

FIG. 6. The isofractional differences, as a percent, for the allowed solutions for the mixing angle θ_{13} in the $P(\nu)\equiv P(\nu_\mu\to\nu_e)$ versus $CP[P(\nu)]\equiv P(\overline{\nu}_\mu\to\overline{\nu}_e)$ plane for the CERN-Frejius project. The parameters are the same as in Fig. 1 with $\Delta m^2_{12}=5\times10^{-5}$ eV^2. The dashed ellipses are labeled $CP^{(\pm)}_{\sin^2 2\theta_{13}}$ to show the relevant size of $\sin^2 2\theta_{13}$ for this figure.

and one would have expected that there is no ambiguity in the determination of the sign of Δm^2_{13}. Hence there is a ''no-go theorem'' for the determination of the sign of Δm^2_{13} by a single T violation measurement. The possible cases in which the ''theorem'' is circumvented are, as mentioned in the Introduction, (a) one of the solutions is excluded, for example, by the CHOOZ constraint, or (b) some additional information, such as energy distribution of the appearance electrons or another T violation measurement with different parameters, is added.

IV. PARAMETER DEGENERACY IN *CP*-VIOLATION MEASUREMENTS

We now turn to the analytic treatment of the parameter degeneracy in CP-violation measurements. We proceed in an analogous way to the analytic treatment of T violation given in Sec. III.

We start with the four basic CP equations for small $\sin\theta_{13}$:

$$P(\nu)_+ = X_+\theta^2 + Y_+\theta\cos\left(\delta+\frac{\Delta_{13}}{2}\right)+P_\odot,$$

$$CP[P(\nu)]_+ \equiv \overline{P}(\nu)_+ = \overline{X}_+\theta^2 + \overline{Y}_+\theta\cos\left(\delta-\frac{\Delta_{13}}{2}\right)+P_\odot,$$

$$P(\nu)_- = X_-\theta^2 + Y_-\theta\cos\left(\delta-\frac{\Delta_{13}}{2}\right)+P_\odot, \qquad (25)$$

$$\mathrm{CP}[P(\nu)]_- \equiv \overline{P}(\nu)_- = \overline{X}_-\theta^2 + \overline{Y}_-\theta\cos\left(\delta+\frac{\Delta_{13}}{2}\right)+P_\odot$$

where $X_\pm$ and $Y_\pm$ are given in the Appendix. As before, $P_\odot$ indicates the term which is related with solar neutrino oscillations, $\Delta_{13}\equiv|\Delta m^2_{13}|L/2E$, the $\pm$ here refers to the sign of Δm^2_{13} and θ is an abbreviation of $\theta_{13}\simeq s_{13}$.

Note that there exist relations among coefficients;

$$X_\pm \equiv X(\pm\Delta m^2_{13}, a), \qquad (26)$$

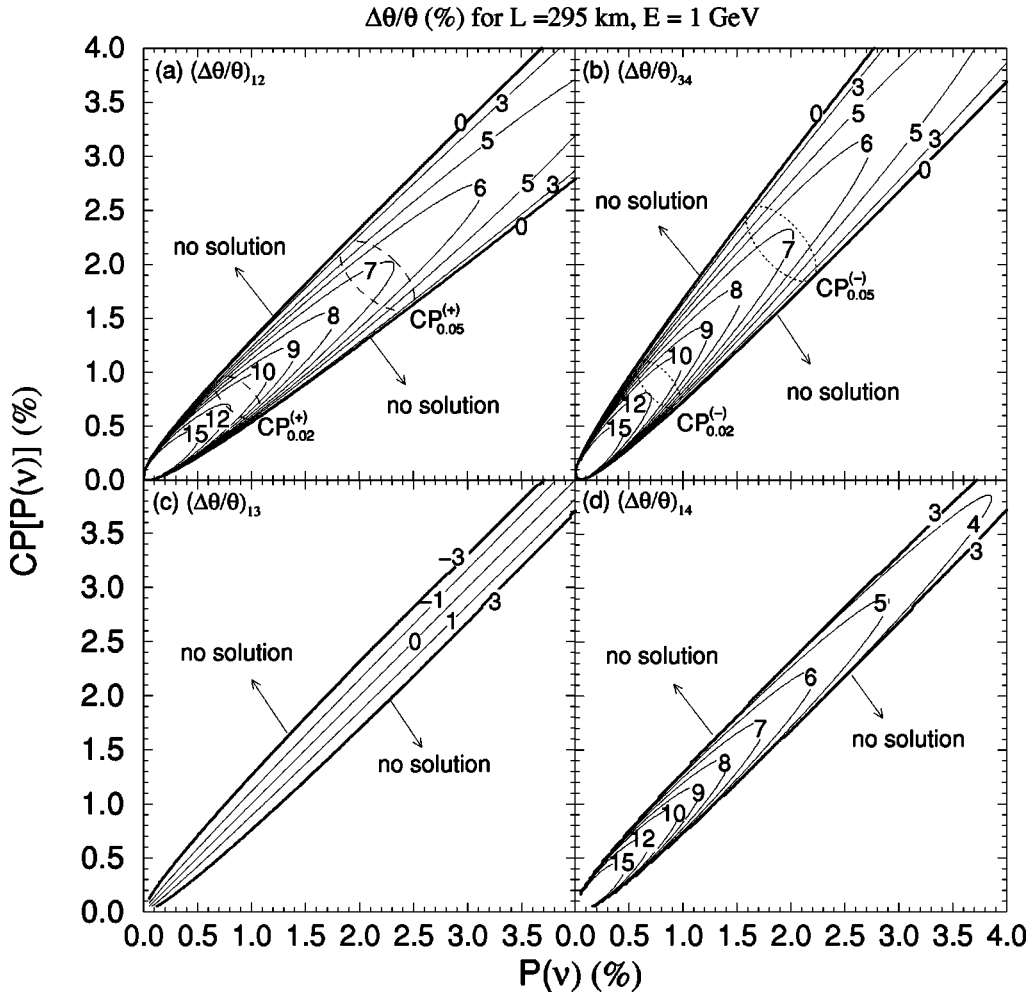

FIG. 7. The isofractional differences, as a percent, for the allowed solutions for the mixing angle θ_{13} in the $P(\nu)\equiv P(\nu_\mu\to\nu_e)$ versus $CP[P(\nu)]\equiv P(\bar{\nu}_\mu\to\bar{\nu}_e)$ plane for the JHF-SK project. The parameters are the same as in Fig. 1 with $\Delta m^2_{12}=5\times10^{-5}$ eV^2. The ellipses are labeled as in Fig. 6.

$$\bar{X}_\pm = X(\pm\Delta m^2_{13}, -a). \tag{27}$$

In leading order in $\Delta m^2_{12}/\Delta m^2_{13}$, there exist further relations,

$$X_+ = \bar{X}_- \text{ and } X_- = \bar{X}_+ \tag{28}$$

which follows from the *CP-CP* relation [12] (see the Appendix). Finally, it follows under the approximation of Cervera *et al.* [21] that

$$Y_+ = -\bar{Y}_-, \quad Y_- = -\bar{Y}_+. \tag{29}$$

We fully utilize the symmetry relationships (28) and (29) in the unified treatment of the same-sign and the mixed-sign degeneracies. The basic equations (25) can be solved for generic mixed-sign situations as

$$\theta_1 = \sqrt{\frac{P-P_\odot}{X_+}} - \frac{Y_+}{2X_+}\cos\left(\delta_1 + \frac{\Delta_{13}}{2}\right), \tag{30}$$

$$\theta_1 = \sqrt{\frac{\bar{P}-P_\odot}{X_-}} + \frac{Y_-}{2X_-}\cos\left(\delta_1 - \frac{\Delta_{13}}{2}\right), \tag{31}$$

$$\theta_3 = \sqrt{\frac{P-P_\odot}{X_-}} - \frac{Y_-}{2X_-}\cos\left(\delta_3 - \frac{\Delta_{13}}{2}\right), \tag{32}$$

$$\theta_3 = \sqrt{\frac{\bar{P}-P_\odot}{X_+}} + \frac{Y_+}{2X_+}\cos\left(\delta_3 + \frac{\Delta_{13}}{2}\right). \tag{33}$$

The solutions of these equations are

$$\sin\delta_{1,2} = \frac{1}{D}\left[-C^{(+)}\sin\frac{\Delta_{13}}{2}\Delta P_+ \pm C^{(-)}\cos\frac{\Delta_{13}}{2}\sqrt{D-(\Delta P_+)^2}\right], \tag{34}$$

$$\sin\delta_{3,4} = \frac{1}{D}\left[-C^{(+)}\sin\frac{\Delta_{13}}{2}\Delta P_- \mp C^{(-)}\cos\frac{\Delta_{13}}{2}\sqrt{D-(\Delta P_-)^2}\right], \tag{35}$$

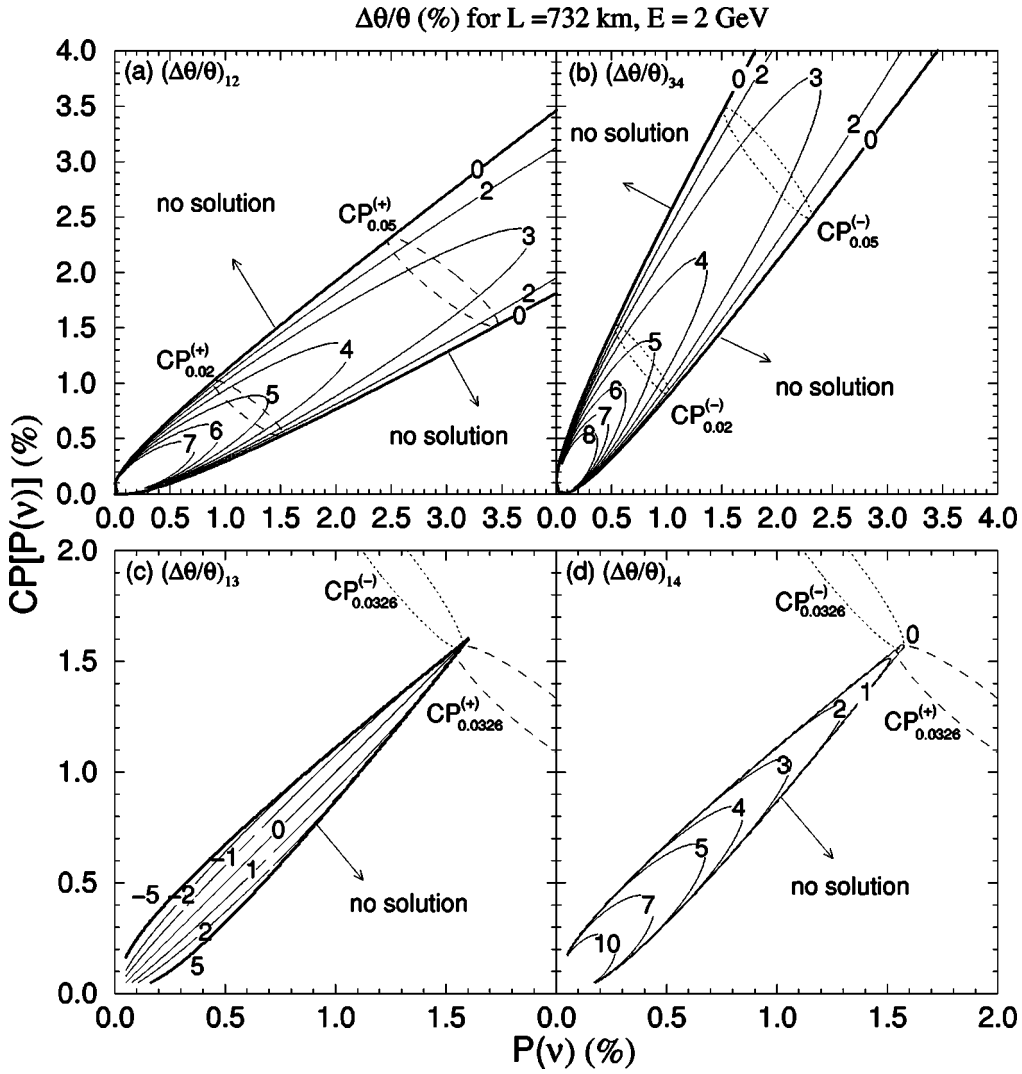

FIG. 8. The isofractional differences, as a percent, for the allowed solutions for the mixing angle θ_{13} in the $P(\nu)\equiv P(\nu_\mu\to\nu_e)$ versus $CP[P(\nu)]\equiv P(\bar{\nu}_\mu\to\bar{\nu}_e)$ plane for the Fermilab-NUMI project. The mixed-sign fractional differences $(\Delta\theta/\bar{\theta})_{13\text{ and }14}$ terminate at around $P=CP[P]\approx 1.6\%$ because above this probability the sign of Δm^2_{13} is determined, as discussed in the text. The critical value of P ($\approx 1.6\%$) and $\sin^2 2\theta_{13}$ (≈ 0.033) can be calculated from Eqs. (49) and (50). The parameters are the same as in Fig. 1 with $\Delta m^2_{12}=5\times 10^{-5}$ eV^2. The ellipses are labeled as in Fig. 6.

$$\theta_{1,2}=\frac{1}{2D^{(-)}}\left[\frac{\sqrt{(P-P_\odot)X_+}}{Y_+}+\frac{\sqrt{(\bar{P}-P_\odot)X_-}}{Y_-}+\sin\delta_{1,2}\sin\frac{\Delta_{13}}{2}\right], \tag{36}$$

$$\theta_{3,4}=\frac{1}{2D^{(-)}}\left[\frac{\sqrt{(P-P_\odot)X_-}}{Y_-}+\frac{\sqrt{(\bar{P}-P_\odot)X_+}}{Y_+}-\sin\delta_{3,4}\sin\frac{\Delta_{13}}{2}\right], \tag{37}$$

where

$$D\equiv C^{(+)2}\sin^2\left(\frac{\Delta_{13}}{2}\right)+C^{(-)2}\cos^2\left(\frac{\Delta_{13}}{2}\right), \tag{38}$$

$$C^{(\pm)}\equiv\frac{1}{2}\left(\frac{Y_+}{X_+}\mp\frac{Y_-}{X_-}\right), \tag{39}$$

$$D^{(\pm)}\equiv\frac{1}{2}\left(\frac{X_+}{Y_+}\mp\frac{X_-}{Y_-}\right), \tag{40}$$

$$\Delta P_\pm\equiv\sqrt{\frac{P-P_\odot}{X_\pm}}-\sqrt{\frac{\bar{P}-P_\odot}{X_\mp}}. \tag{41}$$

The sign in Eq. (35) is determined relative to Eq. (34) so that it reproduces the pair of degenerate solutions in the case of a precisely determined value of θ_{13} [12]. It should be noticed that provided $\sqrt{D-(\Delta P_\pm)^2}$ is real the constraint $|\sin\delta_i|\leqslant 1$ is satisfied automatically in Eqs. (34) and (35).

Let us focus first on the features of the same-sign degenerate solution. The set $(\theta_i,\ \delta_i)$ with $i=1,2$ $(i=3,4)$ de-

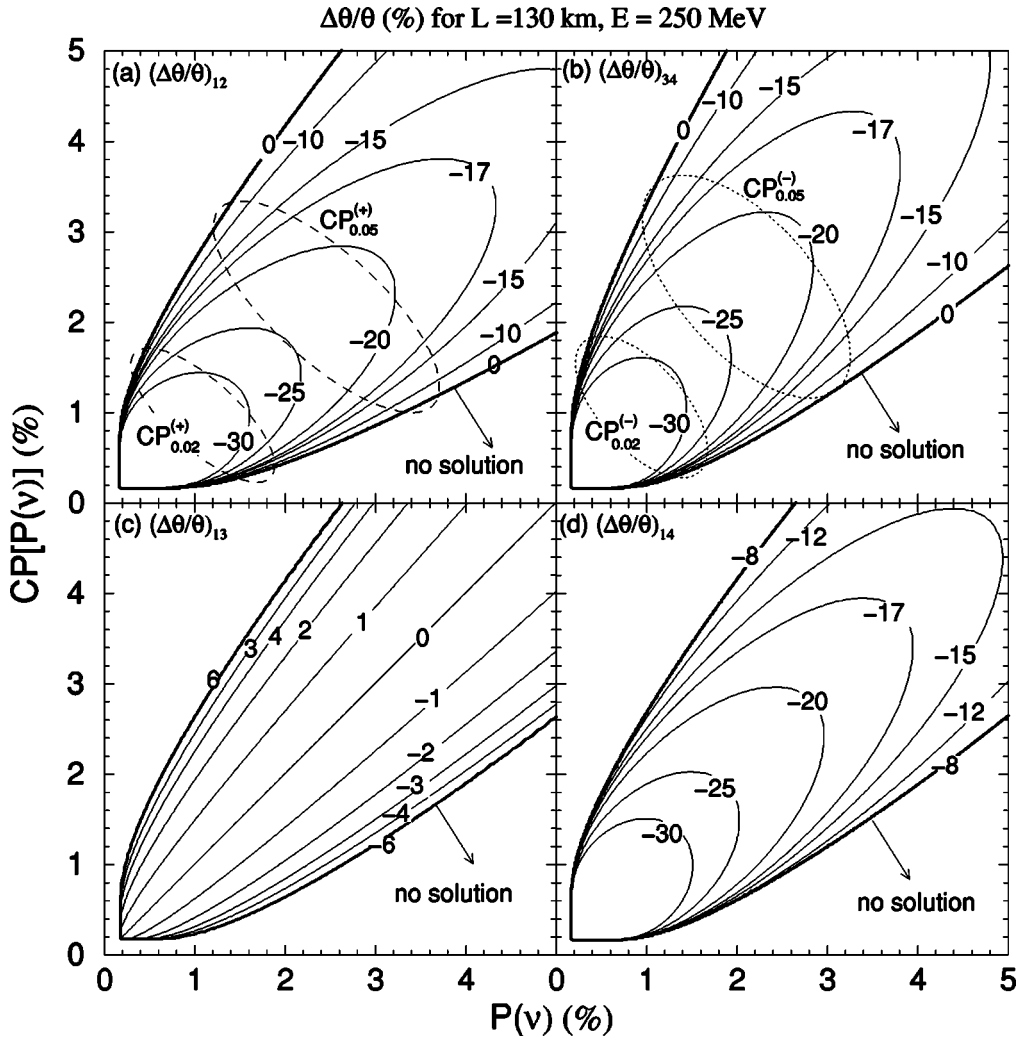

FIG. 9. The isofractional differences, as a percent, for the allowed solutions for the mixing angle θ_{13} in the $P(\nu)\equiv P(\nu_\mu\rightarrow\nu_e)$ versus $CP[P(\nu)]\equiv P(\overline{\nu}_\mu\rightarrow\overline{\nu}_e)$ plane for the CERN-Frejius project. The parameters are the same as in Fig. 1 except for the solar Δm^2_{12} which is set to 1×10^{-4} eV^2 for this plot. The ellipses are labeled as in Fig. 6.

scribes two degenerate solutions with positive (negative) Δm^2_{13} for given values of P and $\overline{P}$. Of course, they reproduce the relationships obtained by Burguet-Castell *et al.* in [9]:

$$\sin\delta_2-\sin\delta_1=-2\left(\frac{\sin\delta_1+z\cos\delta_1}{1+z^2}\right), \tag{42}$$

$$\theta_2-\theta_1=\left(\frac{\sin\delta_1+z\cos\delta_1}{1+z^2}\right)\left(\frac{C^{(+)2}-C^{(-)2}}{C^{(-)}}\right)\sin\left(\frac{\Delta_{13}}{2}\right), \tag{43}$$

where

$$z=\frac{C^{(+)}}{C^{(-)}}\tan\left(\frac{\Delta_{13}}{2}\right). \tag{44}$$

Let us illuminate how the relative phases between δ's between these degenerate solutions can be obtained in a transparent way. Toward the goal we first calculate $\cos\delta_i$. $\cos\delta_{1,2}$ and $\cos\delta_{3,4}$ can be obtained from Eqs. (34) and (35), respectively, by replacing of $C^{(\pm)}$ by $\mp C^{(\mp)}$ and $\sin\Delta_{13}/2$ by $\cos\Delta_{13}2$ and vice versa. One can show by using these results that

$$\cos(\delta_1+\delta_2)=\cos(\delta_3+\delta_4)=\frac{1-z^2}{1+z^2}, \tag{45}$$

which implies that

$$\delta_2=\pi-\delta_1+\arccos[(z^2-1)/(z^2+1)],$$

$$\delta_4=\pi-\delta_3+\arccos[(z^2-1)/(z^2+1)]. \tag{46}$$

Thus in the allowed region of biprobability space δ_2 (δ_4) differs from $\pi-\delta_1$ ($\pi-\delta_3$) by a constant, $\arccos[(z^2-1)/(z^2+1)]$, which depends on the energy and path length of the neutrino beam but not on the mixing angle θ. Near the

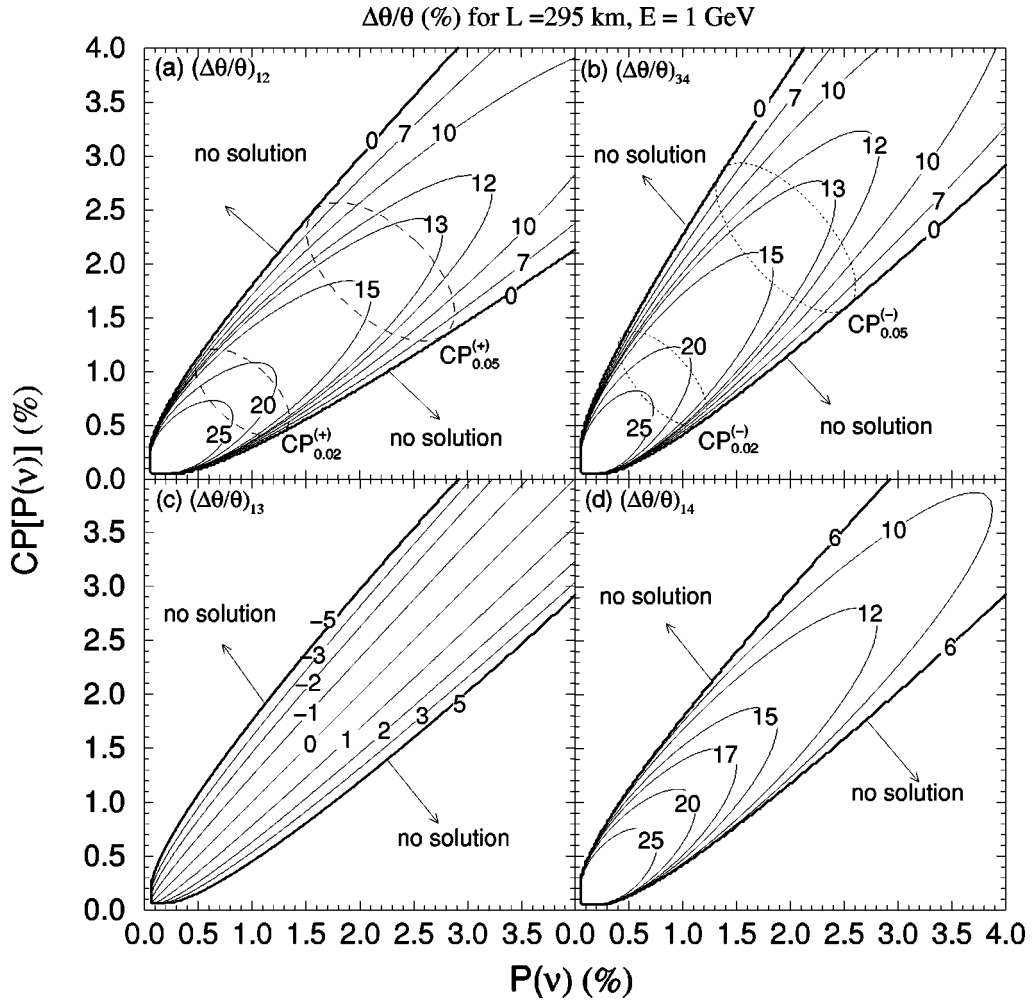

FIG. 10. The isofractional differences, as a percent, for the allowed solutions for the mixing angle θ_{13} in the $P(\nu)\equiv P(\nu_\mu\to\nu_e)$ versus $CP[P(\nu)]\equiv P(\bar{\nu}_\mu\to\bar{\nu}_e)$ plane for the JHF-SK project. The parameters are the same as in Fig. 1 except for the solar Δm^2_{12} which is set to 1×10^{-4} eV^2 for this plot. The ellipses are labeled as in Fig. 6.

oscillation maximum, $z\to\infty$, this constant vanishes so that $\delta_2\simeq\pi-\delta_1$ and $\delta_3\simeq\pi-\delta_4$ as noticed in [9].

For the mixed-sign degenerate solution one can show that

$$\cos(\delta_1-\delta_3)=\frac{(\Delta P_+\Delta P_- -\sqrt{D-\Delta P_+^2}\sqrt{D-\Delta P_-^2})}{D},$$

$$\sin(\delta_1-\delta_3)=\frac{(\Delta P_+\sqrt{D-\Delta P_-^2}+\Delta P_-\sqrt{D-\Delta P_+^2})}{D}. \tag{47}$$

One can show, for example, $\cos(\delta_1-\delta_3)=-1$ and $\sin(\delta_1-\delta_3)=0$ in the $\bar{P}\to P$ limit by noting that $\Delta P_-=-\Delta P_+$ in the limit. It means that $\delta_3=\delta_1+\pi\ (\mathrm{mod}\ 2\pi)$, in agreement with the result obtained in Ref. [12].

The conditions for existence of the same-sign solution are

$$D-(\Delta P_+)^2\geqslant 0 \quad \text{and} \quad D-(\Delta P_-)^2\geqslant 0 \tag{48}$$

for positive and negative Δm^2_{13}, respectively. The condition for existence of the mixed-sign solution is the intersection of the two regions which satisfy the conditions of Eq. (48). An example of the regions satisfying conditions for the existence of the same-sign as well as mixed-sign solutions are depicted in Fig. 1.

The maximum value of P and $\bar{P}$ which allows mixed-sign solutions is determined by $D-(\Delta P_+)^2=D-(\Delta P_-)^2=0$ with $P=\bar{P}$. This occurs for a critical value of P given by

$$P_{\mathrm{crit}}=P_\odot+\frac{X_+X_-D}{(\sqrt{X_+}-\sqrt{X_-})^2}, \tag{49}$$

which can be used to determine the critical value of θ as

$$\theta_{\mathrm{crit}}=\frac{C^{(+)}\sin^2\dfrac{\Delta_{13}}{2}}{2D^{(-)}\sqrt{D}}. \tag{50}$$

There is no degeneracy in the value of θ at this critical point, i.e., $\theta_1=\theta_2=\theta_3=\theta_4$. An example of this can be seen in Fig. 8. At the first peak in the oscillation probability, $\Delta_{13}=\pi$, the value of the critical θ is simply given by

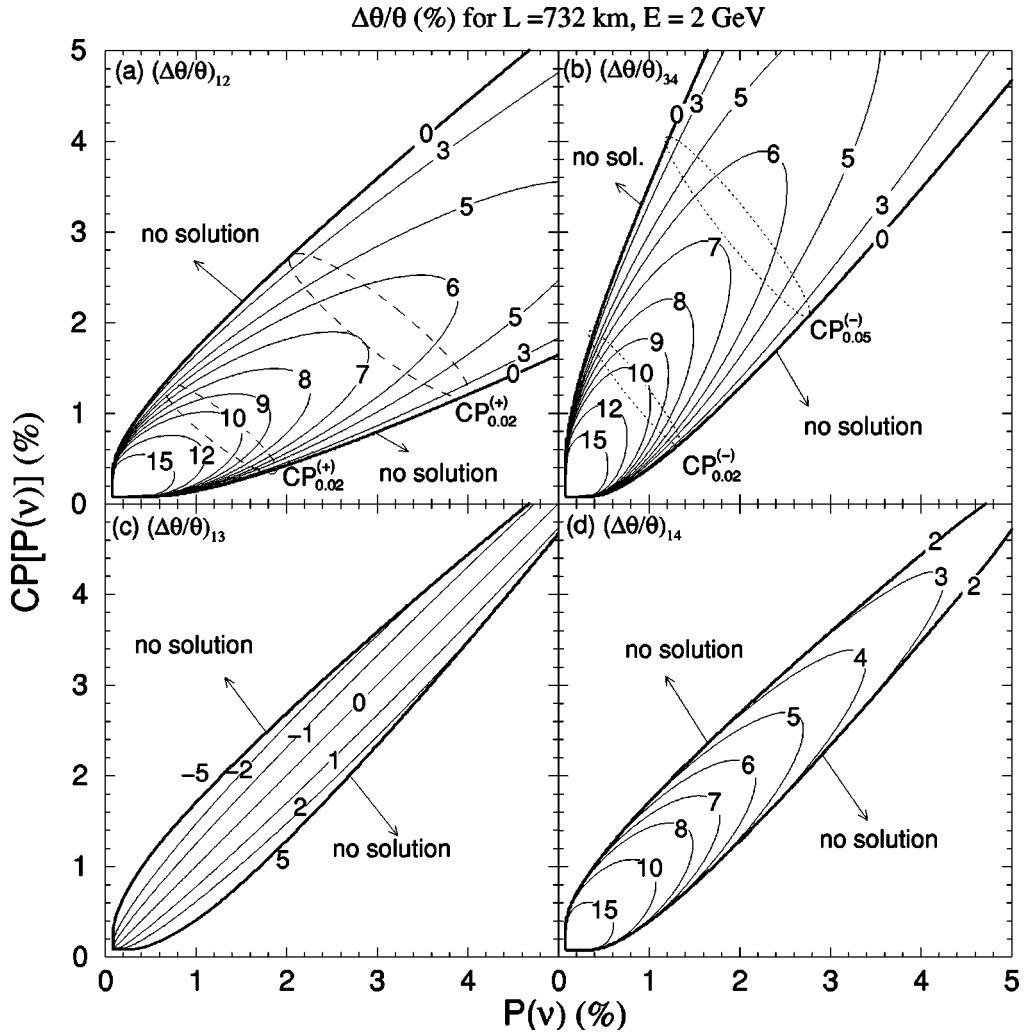

FIG. 11. The isofractional differences, as a percent, for the allowed solutions for the mixing angle θ_{13} in the $P(\nu)\equiv P(\nu_\mu\to\nu_e)$ versus $CP[P(\nu)]\equiv P(\bar{\nu}_\mu\to\bar{\nu}_e)$ plane for the Fermilab-NUMI project. The parameters are the same as in Fig. 1 except for the solar Δm^2_{12} which is set to $1\times10^{-4}\text{eV}^2$ for this plot. The ellipses are labeled as in Fig. 6.

$$\theta_{\text{crit}}(\Delta_{13}=\pi)=\frac{|Y_+|}{\sqrt{X_+}(\sqrt{X_+}-\sqrt{X_-})}. \tag{51}$$

As $\Delta_{13}\to 2\pi$, the critical θ goes to zero and so does the oscillation probabilities P and $\bar{P}$ as this is the position of the first trough in the oscillation probabilities.

In Figs. 6–8 we have plotted the fractional difference, $(\Delta\theta/\bar{\theta})$, see Eq. (18), for the CERN-Frejius, JHF-SK, and Fermilab-NUMI possible experiments using $\nu_\mu\to\nu_e$ and its CP conjugate $\bar{\nu}_\mu\to\bar{\nu}_e$. The regions where this fractional difference is small are regions where the parameter degeneracy inherent in such measurements is only important once the experimental resolution on θ for a fixed solution is of the same size or smaller. Notice that near the boundaries on the allowed region the fractional differences are small for the same sign solutions. For the mixed sign, (1,3), fractional difference plots there is a zero along the diagonal. This is explained by the fact that in our approximation the positive and negative Δm^2_{13} ellipses, for a given θ, intersect along the diagonal. Figures 9–11 are similar to Figs. 6–8 except that the size of solar Δm^2_{12} has been increased by a factor of 2 to 1×10^{-4} eV^2. Notice that the parameter degeneracies problem is more pronounced as the solar Δm^2 is increased. At even larger values of Δm^2_{12}, our approximations become less reliable.

V. SUMMARY AND CONCLUSION

In this paper we have given a complete analytic treatment of the parameter degeneracy issue for θ_{13}, sign of Δm^2_{13} the and the CP, and T violating phase δ that appears in neutrino oscillations. For a given neutrino flavor transition probability and its CP or T conjugate probability we have derived the allowed values of θ_{13}, the sign of Δm^2_{13}, and the CP and T violating phase δ. We have given explicit expressions of degenerate solutions and obtained, among other things, exact formulas for the relationship between solutions of δ's up to the correction of order $(\Delta m^2_{12}/\Delta m^2_{13})^2$.

In general there is a fourfold degeneracy, two allowed

values of θ_{13} for both signs of Δm^2_{13}. This is always true for the T violation measurement whereas for the CP violation measurement the fourfold degeneracy can be reduced to twofold degeneracy if matter effects are sufficiently large, or we live close to the region $\delta \sim \pi/2$ or $3\pi/2$. The significance of matter effects the dependence on the energy of the neutrino beam, the separation between the source and the detector, as well as the density of matter between them. The fractional difference of θ_{13} between the various solutions has been calculated which can be compared with the experimental sensitivity for a given setup to determine whether or not the degeneracy issue is significant or not.

For the possible future experimental setups CERN-Frejius, JHK-SK, and Fermilab-NUMI we have given numerical results for the channel $\nu_\mu \to \nu_e$ and its CP and T conjugate. The CP conjugate being most relevant for these future superbeam experiments. For the CERN-Frejius, JHF-SK, and Fermilab-NUMI experimental setups the parameter degeneracy issue is only relevant once the experimental resolution on the determination of θ_{13} is better than 15%, 10%, and 5% respectively, assuming a transition probability near 1% and a $\Delta m^2_{12} = 5 \times 10^{-5}$ eV^2, see Figs. 6–8. At larger values of Δm^2_{12} the parameter degeneracy issue becomes more important. These iso-fractional difference plots are useful for comparing the sensitivity of different experimental setups, neutrino energy, path length, and experimental sensitivity to this parameter degeneracy issue.

ACKNOWLEDGMENTS

H.M. thanks the Theoretical Physics Department of Fermilab for warm hospitality extended to him through his stay. This work was supported by the Grant-in-Aid for Scientific Research in Priority Areas No. 12047222, Japan Ministry of Education, Culture, Sports, Science, and Technology. Fermilab is operated by URA under DOE contract No. DE-AC02-76CH03000.

APPENDIX

The standard flavor transition probability for neutrino oscillations in the $\nu_\mu \to \nu_e$ channel can be written as

$$P(\nu)_\pm = X_\pm \theta^2 + Y_\pm \theta \cos\left(\delta \pm \frac{\Delta_{13}}{2}\right) + P_\odot, \tag{A1}$$

where the $\pm$ signs in $X_\pm$ and $Y_\pm$ refer to positive or negative values of Δm^2_{13}, θ is an abbreviation for $\sin\theta_{13}$, and $P_\odot$ indicates the terms related to solar neutrino oscillations. For details on the approximations used in deriving this transition probability see Ref. [21]. All other channels used in this paper, $\nu_e \to \nu_\mu$ and $\bar{\nu}_\mu \to \bar{\nu}_e$, can also be expressed with the same variables, see Secs. III and IV.

The coefficients $X_\pm$ and $Y_\pm$ are determined by

$$X_\pm = 4 s^2_{23} \left(\frac{\Delta_{13}}{B_\mp}\right)^2 \sin^2\left(\frac{B_\mp}{2}\right), \tag{A2}$$

$$Y_\pm = \pm 8 c_{12} s_{12} c_{23} s_{23} \left(\frac{\Delta_{12}}{aL}\right)\left(\frac{\Delta_{13}}{B_\mp}\right) \sin\left(\frac{aL}{2}\right) \sin\left(\frac{B_\mp}{2}\right) \tag{A3}$$

$$P_\odot = c^2_{23} \sin^2 2\theta_{12} \left(\frac{\Delta_{12}}{aL}\right)^2 \sin^2\left(\frac{aL}{2}\right) \tag{A4}$$

with

$$\Delta_{ij} \equiv \frac{|\Delta m^2_{ij}| L}{2E} \quad \text{and} \quad B_\pm \equiv |aL \pm \Delta_{13}|, \tag{A5}$$

where $a = \sqrt{2} G_F N_e$ denotes the index of refraction in matter with G_F being the Fermi constant and N_e a constant electron number density in the earth.

Obviously from the above definitions, $X_\pm$ and $Y_\pm$ satisfy the identity

$$\frac{Y_+}{\sqrt{X_+}} = -\frac{Y_-}{\sqrt{X_-}} \tag{A6}$$

which is used throughout this paper.

[1] Kamiokande Collaboration, Y. Fukuda *et al.*, Phys. Lett. B **335**, 237 (1994); Super-Kamiokande Collaboration, Y. Fukuda *et al.*, Phys. Rev. Lett. **81**, 1562 (1998); S. Fukuda *et al.*, *ibid.* **85**, 3999 (2000).

[2] Homestake Collaboration, K. Lande *et al.*, Astrophys. J. **496**, 505 (1998); SAGE Collaboration, J.N. Abdurashitov *et al.*, Phys. Rev. C **60**, 055801 (1999); GALLEX Collaboration, W. Hampel *et al.*, Phys. Lett. B **447**, 127 (1999); Super-Kamiokande Collaboration, S. Fukuda *et al.*, Phys. Rev. Lett. **86**, 5651 (2001); Super-KamioKande Collaboration, S. Fukuda *et al.*, *ibid.* **86**, 5656 (2001); SNO Collaboration, Q.R. Ahmad *et al.*, *ibid.* **87**, 071301 (2001); SNO Collaboration, Q. R. Ahmad *et al.*, *ibid.* **89**, 011301 (2002); SNO Collaboration, Q. R. Ahmad *et al.*, *ibid.* **89**, 011302 (2002).

[3] K2K Collaboration, S.H. Ahn *et al.*, Phys. Lett. B **511**, 178 (2001); K. Nishikawa, Talk presented at XXth International Conference on Neutrino Physics and Astrophysics (Neutrino 2002), 2002, Munich, Germany.

[4] Z. Maki, M. Nakagawa, and S. Sakata, Prog. Theor. Phys. **28**, 870 (1962).

[5] M.B. Smy, hep-ex/0202020; SNO Collaboration, Q.R. Ahmad *et al.*, Phys. Rev. Lett. **89**, 011302 (2002); J.N. Bahcall, M.C. Gonzalez-Garcia, and C. Peña-Garay, J. High Energy Phys. **07**, 054 (2002); V. Barger *et al.*, Phys. Lett. B **537**, 179 (2002); A. Bandyopadhyay *et al.*, *ibid.* **540**, 14 (2002); P.C. de Holanda and A.Yu. Smirnov, hep-ph/0205241; G.L. Fogli *et al.*, Phys. Rev. D **66**, 053010 (2002); M. Maltoni *et al.*, hep-ph/0207227.

[6] S.P. Mikheev and A.Y. Smirnov, Nuovo Cimento Soc. Ital.

Fis., C **9**, 17 (1986); L. Wolfenstein, Phys. Rev. D **17**, 2369 (1978).
[7] CHOOZ Collaboration, M. Apollonio *et al.*, Phys. Lett. B **420**, 397 (1998); CHOOZ Collaboration, M. Apollonio *et al.*, *ibid.* **466**, 415 (1999); see also, Palo Verde Collaboration, F. Boehm *et al.*, Phys. Rev. D **62**, 072002 (2000).
[8] T. Kajita, H. Minakata, and H. Nunokawa, Phys. Lett. B **528**, 245 (2002).
[9] J. Burguet-Castell, M.B. Gavela, J.J. Gomez-Cadenas, P. Hernandez, and O. Mena, Nucl. Phys. **B608**, 301 (2001).
[10] H. Minakata and H. Nunokawa, J. High Energy Phys. **10**, 001 (2001).
[11] V. Barger, D. Marfatia, and K. Whisnant, Phys. Rev. D **65**, 073023 (2002).
[12] H. Minakata, H. Nunokawa, and S.J. Parke, Phys. Lett. B **537**, 249 (2002).
[13] J. Arafune and J. Sato, Phys. Rev. D **55**, 1653 (1997); J. Arafune, M. Koike, and J. Sato, *ibid.* **56**, 3093 (1997); **60**, 119905(E) (1999); H. Minakata and H. Nunokawa, *ibid.* **57**, 4403 (1998); Phys. Lett. B **413**, 369 (1997); **495**, 369 (2000); K. Dick, M. Freund, M. Lindner, and A. Romanino, Nucl. Phys. **B562**, 29 (1999); O. Yasuda, Acta Phys. Pol. B **30**, 3089 (1999); M. Koike and J. Sato, Phys. Rev. D **61**, 073012 (2000); **62**, 079903(E) (2000).
[14] S.J. Parke and T.J. Weiler, Phys. Lett. B **501**, 106 (2001).
[15] H. Minakata and H. Nunokawa, Nucl. Phys. B (Proc. Suppl.) **110**, 404 (2002).
[16] V. Barger, D. Marfatia, and K. Whisnant, Phys. Rev. D **66**, 053007 (2002).
[17] P. Huber, M. Lindner, and W. Winter, hep-ph/0204352.
[18] A. Donini, D. Meloni, and P. Migliozzi, hep-ph/0206034.
[19] J. Burguet-Castell, M.B. Gavela, J.J. Gomez-Cadenas, P. Hernandez, and O. Mena, hep-ph/0207080.
[20] K. Kimura, A. Takamura, and H. Yokomakura, Phys. Lett. B **537**, 86 (2002); Phys Rev. D **66**, 073005 (2002).
[21] A. Cervera, A. Donini, M.B. Gavela, J.J. Gomez-Cadenas, P. Hernandez, O. Mena, and S. Rigolin, Nucl. Phys. **B579**, 17 (2000); **B593**, 731 (2000).
[22] The idea of low-energy conventional ''superbeam'' for measuring leptonic *CP* violation may be traced back to H. Minakata and H. Nunokawa, Phys. Lett. B **495**, 369 (2000); Nucl. Instrum. Methods Phys. Res. A **472**, 421 (2001); J. Sato, *ibid.* **472**, 434 (2001); B. Richter, hep-ph/0008222.
[23] C. Albright *et al.*, hep-ex/0008064; V. Barger, S. Geer, R. Raja, and K. Whisnant, Phys. Rev. D **63**, 113011 (2001); J. Pinney and O. Yasuda, *ibid.* **64**, 093008 (2001).
[24] Y. Itow *et al.*, ''The JHF-Kamioka neutrino project,'' hep-ex/0106019.
[25] MINOS Collaboration, P. Adamson, *et al.*, MINOS Detectors Technical Design Report, Version 1.0, NuMI-L-337, 1998.
[26] OPERA Collaboration, M. Guler, *et al.*, ''OPERA: An Appearance Experiment to Search for Nu/Mu $\leftrightarrow$ Nu/Tau Oscillations in the CNGS Beam. Experimental Proposal,'' CERN-SPSC-2000-028, CERN-SPSC-P-318, LNGS-P25-00, 2000.
[27] H. Murayama and A. Pierce, Phys. Rev. D **65**, 013012 (2002); see also A. de Gouvêa and C. Peña-Garay, *ibid.* **64**, 113011 (2001); V. Barger, D. Marfatia, and B.P. Wood, Phys. Lett. B **498**, 53 (2001); R. Barbieri and A. Strumia, J. High Energy Phys. **12**, 016 (2000).
[28] CERN working group on Super Beams Collaboration, J.J. Gomez-Cadenas *et al.*, hep-ph/0105297.
[29] D. Ayres *et al.*, hep-ex/0210005.